Colloid & Polymer Science Colloid Polym Sci 269:747–763 (1991)

Leading Contribution

Tensile deformation of high strength and high modulus polyethylene fibers

H. van der Werff*) and A. J. Pennings

Department of Polymer Chemistry, University of Groningen, Groningen, The Netherlands

Abstract: The influence of tensile deformation on gel-spun and hot-drawn ultra-high molecular weight polyethylene fibers has been investigated. In high modulus polyethylene fibers no deformation energy is used to break chemical bonds during deformation, and flow is predominantly present next to elastic behavior. Flow is reversible after tensile deformation to small strains, but becomes irreversible when yielding occurs.

Stress relaxation experiments were used to determine the elastic and flow contribution to tensile deformation. A simple quantitative relation could then be derived for the stress-strain curve that directly links yield stress to modulus. Experimental stress-strain curves could be reasonably described by this relation.

Flow during tensile deformation is shown to be correlated with the introduction of the hexagonal phase in crystalline domains. A mechanism of flow is proposed in which, at first, tie molecules or intercrystalline bridges are pulled out of crystalline blocks (reversible), followed by the break-up of crystalline blocks through slip of microfibrils past each other (stress-induced melting, irreversible).

Key words: Tensile deformation; deformation energetics; stress-induced phase transition; chain slip; Polyethylene fibers

1. Introduction

High strength and high modulus fibers from ultra-high molecular weight polyethylene (UHMWPE) can be prepared by gel-spinning and subsequent hot-drawing [1–3]. Tensile strengths up to 7.2 GPa [4, 5] can be achieved and Young's moduli of 264 GPa are reported in this work.

The failure mechanism of these fibers is not yet fully understood. Fiber failure can in general be a result of breaking of chemical bonds [6, 7] or slip of chains past each other [8]. An extensive overview on this subject has been given by Kausch [9]. Recently [10], it was found that at higher temperatures tensile strengths of UHMWPE fibers are limited by a stress-induced orthorhombic-hexagonal phase transition that causes slip of chains. Viscoelastic properties [11] may therefore still play an important role during tensile deformation of high strength and high modulus UHMWPE fibers.

The aim of this work is to investigate the effects of tensile deformation on UHMWPE fibers. Normally, tensile strength, Young's modulus, and strain at break are the only tensile properties considered. Detailed experimental analysis of stress-strain behavior may give insight into the processes that could take place during tensile deformation like, for example, elastic deformation, chain scission, chain slip, formation of cracks, etc. Precise knowledge on these processes is needed as a basis to understand why these important materials in practice cannot achieve the properties they theoretically could have.

2. Experimental

The UHMWPE fibers were prepared according to standard procedures in our laboratory [2, 4, 10]. Polyethylene solutions with different weight percentages polyethylene were prepared

*) Present address: AKZO Research Laboratories, P.O. Box 9300, 6800 SB Arnhem, The Netherlands

in paraffin oil containing 0.5 wt.% anti-oxidant (2,6-di-*t*-butyl-4-methyl-cresol) by stirring at 140 °C until the Weissenberg effect began to occur. These solutions were subsequently homogenized for 48 h under nitrogen atmosphere at 150 °C, after which it was slowly cooled down to room temperature. The solution then has formed a gel which is fed into the spinning apparatus. After a dissolution time of 2 h at 190 °C, the solution was spun at this temperature through a conical die [12] with an outlet diameter of 1 mm at an extrusion speed of 1 m/min. The gel-fibers were wound onto a bobbin at the same speed. The paraffin oil and the anti-oxidant were removed from these fibers by extraction with *n*-hexane. After extraction, the constrained fibers were dried at 50 °C under vacuum for 1 h. The fibers were hot-drawn using a tubular oven at 148 °C in a small flux of nitrogen. Draw ratios were determined by the ratio of the velocity out of and in the oven. The cross-sectional areas of the fibers were determined from weight and length , assuming a density of 1000 kg/m^3.

Two different samples of linear polyethylene Hifax 1900 were used – one with a broad molecular weight distribution ($M_w = 4 \times 10^6$ kg/mol, $M_w/M_n = 20$, referred to as Hifax A), and one with a narrower molecular weight distribution ($M_w = 5.5 \times 10^6$ kg/mol, $M_w/M_n \approx 3$, referred to as Hifax B).

Tensile testing was performed on an Instron 4301 tensile tester equipped with type 2712-002 pneumatic action grips. The flat type grip faces with smooth ground surface were 7.5-mm wide. Gripping force was controlled by adjusting the air pressure in such a way that slip of fibers through the grips did not occur. At this level of the gripping force, however, failure is mostly initiated at the grips, as would be expected for fibrous samples. Normally, fibers were tested using a sample length of 100 mm and a constant crosshead speed of 10 mm/min.

In order to obtain highly accurate stress-strain data, the tensile tester was digitized by installation of the Instron Series IX Automated Materials Testing program. Fibers were then tested at a sample length of 500 mm, constant crosshead speed of 50 mm/min and a sampling rate of 20 points/s.

3. Results and discussion

Cyclic deformations and deformation energetics

Hysteresis during cyclic deformations of viscoelastic materials is a very well known phenomenon [13]. In Fig. 1 two deformation cycles are shown of a UHMWPE fiber from a 2.5 wt.% gel with a draw ratio λ of 60, which corresponds closely to the maximum draw ratio in one step at 148 °C. After the first cycle, the crosshead was returned to its original position and after a recovery period of two minutes the second cycle was recorded.

The hysteresis is clearly non-elastic in the two deformation cycles, i.e., the strain at which the stress becomes zero in the unloading curve is in both cycles larger than the strain at which the

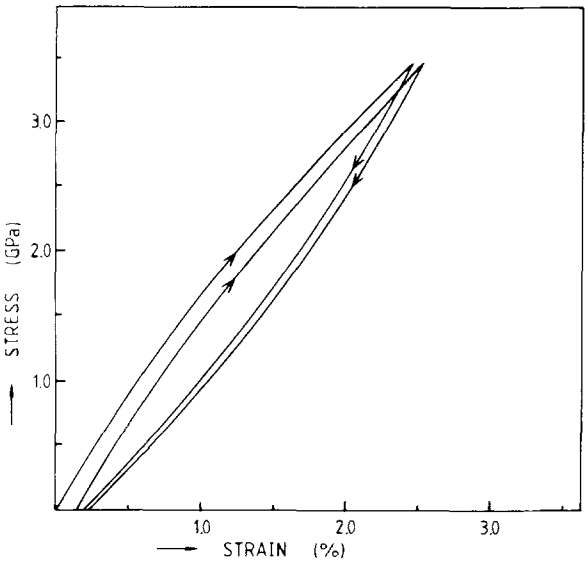

Fig. 1. Two consecutive deformation cycles of an UHMWPE fiber ($\lambda = 60$, 2.5 wt.% Hifax B)

loading cycle started. Comparing the two cycles, one can see that the strain at which the loading curve of the second cycle started is smaller than the strain at which the unloading curve of the first cycle stopped. This indicates that, after unloading to zero stress and zero initial strain, a recovery process must have taken place during which the fiber has contracted. It has been found that in the case of long delay times between two cycles (about 1 to 2 days, which corresponds to a recovery time of about 3000 times longer than loading and unloading time), the stress-strain characteristics of the first cycle are totally recovered so that the second cycle becomes completely identical to the first. This has been confirmed on fibers that have a small strain at break (3–4%). The fact that this recovery process takes place also proves that the apparent elongation of a sample after a deformation cycle is not caused by slip of the sample through the clamps of the tensile tester. If that would be the case, the initial stress-strain behavior could never be recovered.

This means that the process that causes the non-elastic hysteresis during a cyclic deformation is reversible and that no plastic deformation, i.e., a permanent elongation after deformation occurs. Deformation of a fiber causes a recoverable, time-dependent change from its initial morphology. This is in accordance with results of studies on tensile

creep and recovery [14, 15] on polyethylenes with lower molecular weight. It was found that these materials showed an apparent critical stress below which there was no detectable permanent creep. This critical stress increased with molecular weight.

The fact that the morphology of a fiber must have changed during cyclic deformation is also clear if one compares the various energies of the deformation process. The energy U needed to elongate a fiber from a strain ε_1 to a strain ε_2 is

$$U = \int_{L_1}^{L_2} F\,dL = V \int_{\varepsilon_1}^{\varepsilon_2} \sigma\,d\varepsilon\,, \qquad (1)$$

where L is the fiber length, V is the fiber volume, F the tensile force, and σ the tensile stress. From Fig. 1 it can be seen that the area under the first loading curve is larger than the area under the first unloading curve. The difference between them is the dissipated energy. The same holds for the second cycle, but this dissipated energy is smaller than that in the first cycle. The energy recovered under the unloading curve however is nearly the same for both cycles. The fact that total deformation energy and the dissipated energy differ between the two cycles indicates that the properties of the fiber have changed during deformation.

In general, the following energies can be determined on the basis of cyclic deformation:

- U_{tot}: total deformation energy (the area under the loading curve);
- $U_{elastic}$: apparent elastic energy (the area under the unloading curve);
- U_{dis}: dissipated energy ($U_{tot} - U_{elastic}$).

By performing a second deformation cycle, the dissipated energy can be split into two parts:

- $U_{dis,2}$: dissipated energy in the second cycle, i.e. the energy that can be dissipated again immediately;
- $U_{dis,\Delta}$: dissipated energy in the first cycle that can not be dissipated again (difference in U_{dis} between the first and second cycle).

The amount of $U_{dis,\Delta}$ is a measure of how much the fiber structure has changed. When this value is zero (which is the case when the recovery period between the two cycles is sufficiently long), the stress-strain behavior in both cycles is identical.

These energies have been determined for the fiber shown in Fig. 1. The plot of the energies as a function of strain in the first cycle, is given in Fig. 2. At the largest strain at which the energies could be determined 72% of the deformation energy is still elastic. This percentage goes up for smaller strains, although there is no region where the fiber is completely elastic. The highest value measured was 79% elastic energy at a strain of 1.09%. From the dissipated energies, $U_{dis,2}$ is substantially higher than $U_{dis,\Delta}$. This means that, on this time-scale, most of the dissipated energy is dissipated as heat and that only a relatively small amount is used to temporarily change the structure of the fiber. However, when the change of structure is recovered in time this small amount of energy will also be gradually dissipated as heat. All energies rise smoothly with increasing strain. Very similar plots can be found for all fibers having a strain at a break of 3 to 4.5%. Quantitatively, it can be said that fibers having lower draw ratios show a smaller percentage of elastic energy at the same value of U_{tot}. The total deformation energy up to break is about the same for all fibers. Fibers spun from different gels, but having the same draw ratio (like, for example, $\lambda = 30$ from a 2.5 wt.% and a 6.0 wt.% gel) give practically the same energy plots.

The amount of dissipated energy per volume U_{dis} can be related to an elongational viscosity η

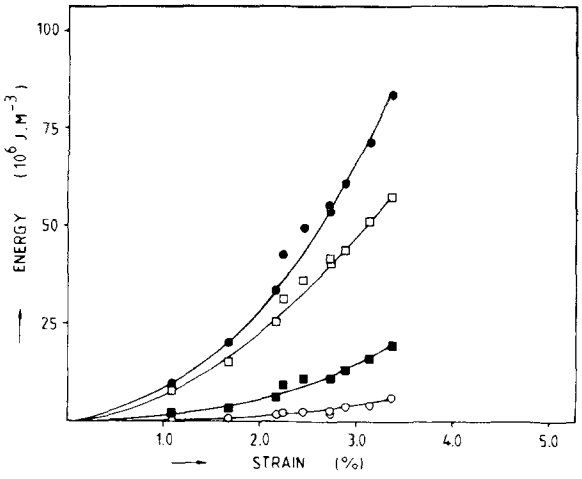

Fig. 2. Deformation energies versus tensile strain of an UHMWPE fiber ($\lambda = 60$, 2.5 wt.% Hifax B). ●: U_{tot}, □: $U_{elastic}$, ■: $U_{dis,2}$, ○: $U_{dis,\Delta}$

through the following relation:

$$U_{dis} = \eta \cdot (\dot{\varepsilon})^2 \cdot t \,, \qquad (2)$$

where $\dot{\varepsilon}$ is the deformation rate and t the elapsed time. The fiber in Fig. 2 has dissipated 26.3 $\times 10^6$ J/m^3 at a cycle strain of 3.37% ($\dot{\varepsilon} = 1.67 \times 10^{-3}$ s^{-1}, therefore $t = 40.4$ s). Using (2), one can calculate $\eta = 2.33 \times 10^{11}$ N·m^{-2}·s. This value compares very well with elongational viscosities of UHMWPE fibers at higher temperatures [16], and this viscosity must then be assigned to disordered domains in the fiber morphology. Such domains do not seriously contribute to the tensile stress, but elongation and contraction of these viscous regions results into dissipation of deformation energy as heat.

Fibers that yield during deformation, give rise to a very different behavior. Generally, these fibers have a low draw ratio relative to the maximum draw ratio. Figure 3 shows the various energies versus strain for a $\lambda = 15$ fiber spun from a 2.5 wt.% gel. In the stress-strain curve of the fiber the stress gradually increases with strain up to about 7% and then levels off abruptly (yielding). At low strains the relative values of the energies resemble those presented in Fig. 2. At higher strains the elastic energy levels off and $U_{dis,\Delta}$ rises steeply. $U_{dis,2}$ also rises with increasing strain, but less steeply. After the point where yield starts the percentage of $U_{dis,\Delta}$ is highest. It was found that by yielding plastic deformation is introduced. After the fiber of Fig. 3 had been strained to 8% in the first cycle, the crosshead was returned to its original position, and after 64 h the second cycle was carried out. The sample then showed a permanent elongation of 1.9% of its initial length. It can be concluded therefore that the rise of $U_{dis,\Delta}$ at the beginning of yielding must be attributed to energy put into plastic deformation. The elastic energy levels off, because the stress hardly rises after the yield point and the elastic part of the fiber morphology is not being elongated anymore. The increase in strain after the beginning of the yield must be solely caused by plastic flow that may lead to an irrecoverable elongation of the fiber, and irreversible dissipation of deformation energy.

The results of the energy analysis on UHMWPE fibers, as presented in Figs. 2 and 3, differ markedly from similar studies by Frank and Wendorff on polyamide fibers [17, 18]. From ESR experiments they showed that deformation above a critical

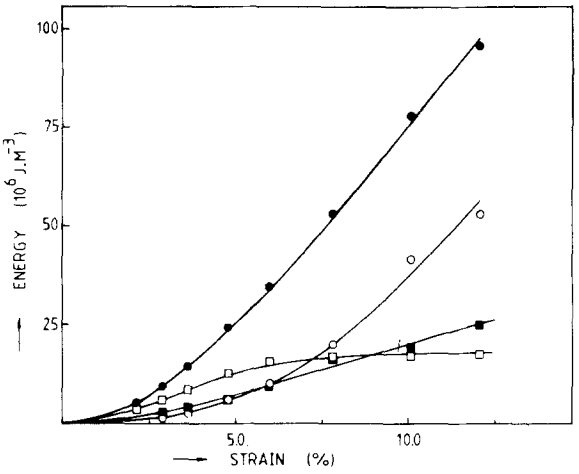

Fig. 3. Deformation energies versus tensile strain of an UHMWPE fiber ($\lambda = 15$, 2.5 wt.% Hifax B). ●: U_{tot}, □: $U_{elastic}$, ■: $U_{dis,2}$, ○: $U_{dis,\Delta}$

strain level gave rise to chain rupture events. By tensile deformation the stress-strain behavior of the polyamide fibers was irreversibly changed and the irreversible dissipation of energy during deformation was accounted for in terms of energy release after chain ruptures. The breaking of chains was confirmed by a decrease in molecular weight.

From the results of the preceding energy analysis of UHMWPE fibers, one must conclude that during tensile deformation of these fibers, even close to breaking strain, no detectable amount of chains is broken. Irreversibly dissipated energy is not present, except for yielding fibers where this energy has to be associated with work needed for plastic deformation. Stoeckel et al. [19] have found no relevant decrease in the molecular weight of a polyethylene sample after it had been fractured in tensile deformation. ESR studies on UHMWPE fibers in our laboratory have shown that under tensile stress no relevant amount of free radicals due to chain rupture could be detected [20]. Small angle x-ray scattering studies on strained UHMWPE fibers [21] show no detection of void formation, even at strains close to break. Although Zhurkov [22] found considerable increase in scattering intensity while straining films of oriented polyethylene of ordinary molecular weight up to break, this void formation may be attributed to the opening of spaces between lamellae [23]. All these studies, together with the results from this work, indicate that tensile deformation of high modulus

and high strength UHMWPE fibers does not involve significant breaking of chains. Viscoelastic processes play a major role, as will be shown by repeated cyclic loading.

In Fig. 4 three loading cycles are presented for a $\lambda = 15$ fiber from a 6.0 wt.% gel (a non-yielding fiber at the applied deformation rate). In cycle A the fiber is strained up to 1.20 GPa stress, after which the crosshead speed is reversed. When the tensile stress has become zero, the crosshead speed is again immediately reversed and, in a similar way, a number of cycles is performed. Cycle B is the 35th cycle. If one compare cycles A and B, it is clear that cycle A corresponds to cycles as shown in Fig. 1, and that cycle B is distinctly different. First of all, the tangent modulus in the loading curve of B does not decrease monotonically as in A, but goes, after an initial decrease, through a minimum and then increases again. The shapes of the unloading curves in A and B are similar. The end of the unloading curve in B, however, comes very close to the beginning of its loading curve. The hysteresis has almost become elastic and the dissipated energy in cycle B is much less than in cycle A. After performing cycle B, the crosshead was returned to the position corresponding to zero initial strain and the sample was allowed to recover during 75 min., before cycle C (the 36th) was recorded.

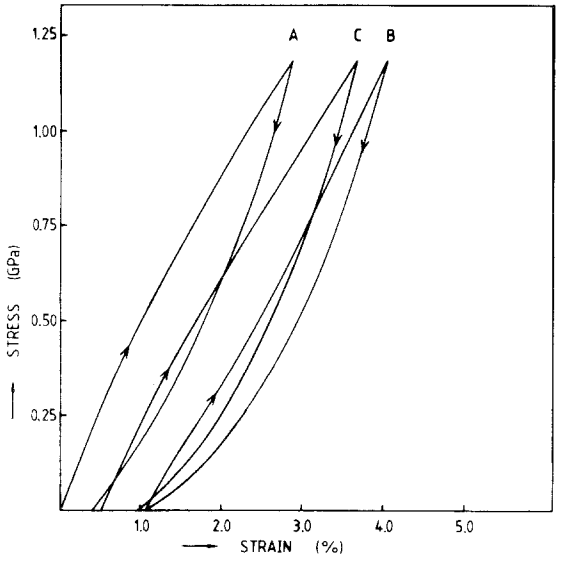

Fig. 4. Three consecutive deformation cycles up to 1.20 GPa of an UHMWPE fiber ($\lambda = 15$, 6.0 wt.% Hifax B). A: first cycle, B: 35th cycle, C: 36th cycle. Recovery time between cycle B and C is 75 min

The stress-strain behavior changes dramatically after recovery. The beginning of the loading curve of C has shifted to about halfway in between the beginnings of A and B: the sample must have contracted itself. Typically, the hysteresis has again become non-elastic after recovery, and the energy dissipated in cycle C is much larger than in cycle B. Furthermore, the shape of the loading curve in C again resembles that of cycle A.

One can qualitatively comprehend this behavior if a fiber is assumed to consist of many viscous elements making up a spectrum of characteristic times with respect to contraction (like different Voigt elements [11]). In the first deformation cycle A, many viscous elements with long contraction times relative to the unloading time cannot contract during the unloading time although they have contributed to elongation in the loading curve. Hysteresis therefore results. After several cycles, only the elements with contraction times equal to or smaller than the cycle time will follow the cyclic elongation and contraction. Hysteresis then becomes almost completely elastic, like in cycle B (the 35th). The dissipated energy will then also go down, because less viscous elements elongate and contract during a cycle, thus reducing energy lost into the friction caused by these movements; the system thus becomes relatively more elastic. After a long recovery time the "slow" elements will have more or less contracted and may again participate in the loading of cycle C and the dissipated energy goes up. This explains the contraction of the fiber and the change of the loading curve during recovery and the similarity of the unloading curves (in all cycles only the relatively fast elements will determine the shape of the unloading curve).

The relative shift of the maximum strain during cyclic deformation up to different stress levels is plotted versus the number of cycles in Fig. 5. From this, it is evident that the shift of maximum strain becomes relatively larger at higher stress levels. At a stress level close to break the shift becomes especially dramatic and may lead to breakage of the fiber (indicated by the × in Fig. 5). This type of behavior is obviously related to creep, for it reflects the property of increasing strain at a given stress level.

Very similar behavior is found when cyclic deformations up to a given strain level are examined. In Fig. 6 three cycles are shown for the same fiber as in Figs. 4 and 5, deformed cyclically up to 5.0%

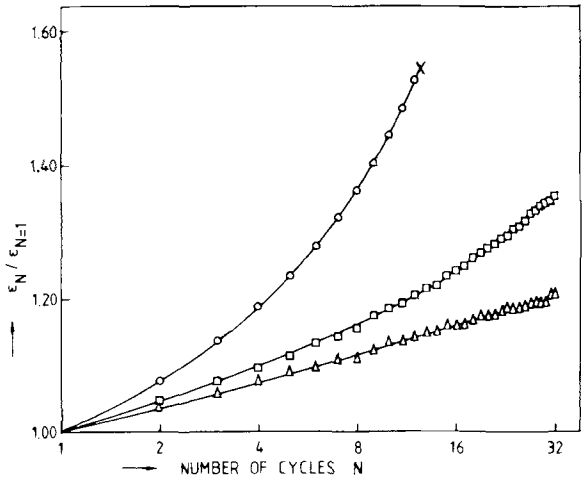

Fig. 5. Relative shift of maximum strain versus the number of deformation cycles up to three different stress levels of an UHMWPE fiber ($\lambda = 15$, 6.0 wt.% Hifax B). Δ = 0.77 GPa, □: 1.20 GPa, ○: 1.64 GPa, ×: fiber failure

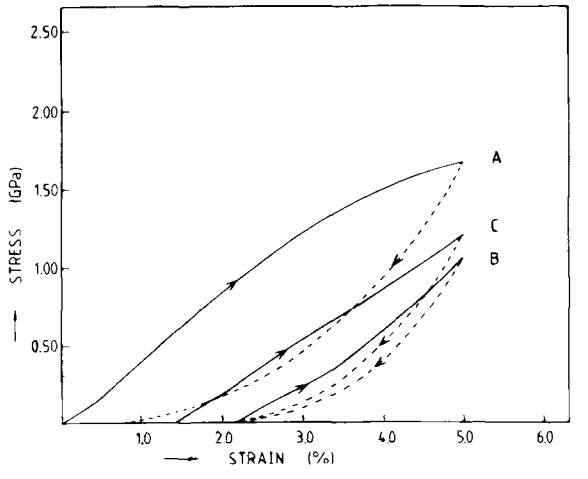

Fig. 6. Three consecutive deformation cycles up to 5.0 % strain of an UHMWPE fiber ($\lambda = 15$, 6.0 wt.% Hifax B). A: first cycle, B: 35th cycle, C: 36th cycle. Recovery time between cycle B and C is 60 min

initial strain. Cycle A is the first cycle, B the 35th. Clearly, the stress decreases at 5.0% initial strain, and the shape of the loading curve has changed from A to B, in the same way as described in Fig. 4. The hysteresis in B has become almost elastic, and the energy dissipated in the cycle has gone down drastically. After a recovery time of 60 min. cycle C was recorded. Again the recovery has resulted in a change of the loading curve, increase of dissipated energy, and contraction of the fiber. The qualitative explanation given for the behavior presented in Fig. 4 is also valid here.

The relative decrease of the maximum stress for different strain levels as a function of the number of cycles is given in Fig. 7. The decrease of the stress becomes relatively larger at larger strains. As a function of the number of cycles, plotted on a logarithmic scale, the stress decreases almost linearly. In this case, such behavior must be related to stress relaxation, i.e., the tendency to lower stress at a given strain level. It needs to be emphasized that all the properties displayed in Figs. 4–7 are qualitatively applicable to all high strength and high modulus UHMWPE fibers, although only one fiber with a low draw ratio was being considered for sake of clarity. Quantitaively, these properties become less pronounced for fibers with higher draw ratios, but are still present.

The results of the cyclic deformations show that UHMWPE fibers in no way exhibit purely elastic behavior. Properties, inherent to viscoelastic materials like creep and stress relaxation play a prominent role in the tensile deformation, even for fibers having very high crystallinity (~ 90%) and initial modulus (up to 264 GPa (for a $\lambda = 170$ fiber from a 1.5 wt.% Hifax B gel), which is about 75% of the ultimate modulus [24]). This observation has already been made by Ward et al. [25] in a study on

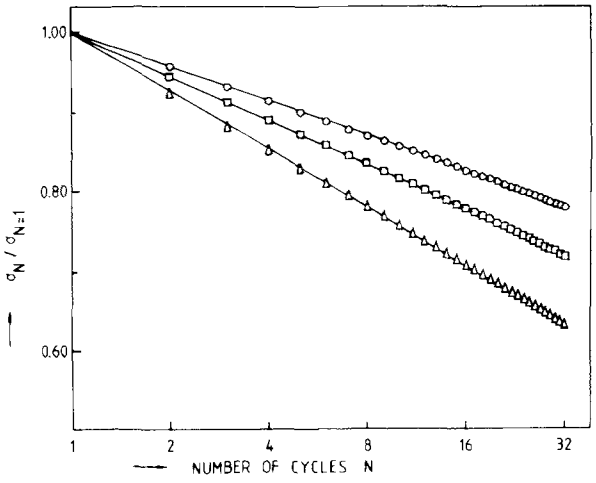

Fig. 7. Relative decrease of maximum stress versus the number of deformation cycles up to three different stress levels of an UHMWPE fiber ($\lambda = 15$, 6.0 wt.% Hifax B). ○: 3.0%, □: 4.0%, Δ = 5.0%

creep of UHMWPE fibers prepared in our laboratory. They find that, in terms of a critical stress below which no permanent deformation can be observed, these fibers show a lower value than any of the other filaments studied.

In order to understand the deformation behavior of UHMWPE fibers, viscoelastic properties have to be taken into account and will therefore be studied in the following section.

Stress relaxation

During stress relaxation, plastic flow changes the structure of a fiber and thus reduces stress at a given strain. Stress relaxation has been extensively studied [11, 13]. Kubát and coworkers have reported several studies on stress relaxation on polyethylene [26–29]. In a typical stress relaxation experiment, the sample is elongated to a certain strain and the subsequent relaxation of stress is being followed over substantial period of time until stress reaches a stationary level. Relations are being derived to describe stress relaxation over a wide range of time and stress. The approach to stress relaxation to be used in this study is different and will be explained using Fig. 8.

Figure 8 schematically shows the stress-time curve of a stress relaxation experiment on UHMWPE fibers. The fiber is elongated using a constant crosshead speed until time t, where the displacement of the crosshead is stopped. From then on the stress relaxes. All experiments show that, at time t, there is an instantaneous and definite stress relaxation rate $\dot{\sigma}_{\text{relax}}(t)$ (the dot denotes the time derivative). The relaxation process obviously does not start at time t, but must already have been present during the elongation process. The stress rate in the loading curve at time t, $\dot{\sigma}(t)$, must therefore have resulted from two different stress rate mechanisms. The stress relaxation rate $\dot{\sigma}_{\text{relax}}(t)$ must have been counterbalanced by another, oppositely directed stress rate mechanism $\dot{\sigma}_c(t)$ (the subscript c is used to denote the counterbalancing effect), in order to result in the stress rate $\dot{\sigma}(t)$ in the loading curve. In formula this is

$$\dot{\sigma}(t) = \dot{\sigma}_c(t) + \dot{\sigma}_{\text{relax}}(t) \,, \tag{3}$$

with: $\dot{\sigma}(t), \dot{\sigma}_c(t) > 0$

$\dot{\sigma}_{\text{relax}}(t) < 0$

for the situation depicted in Fig. 8.

In Fig. 9 the various stress rates are plotted versus the tensile stress, at which the crosshead was stopped. For every measurement, a new piece of fiber was mounted in the tensile tester. The fiber used was spun from a 2.5 wt.% gel and hot-drawn to $\lambda = 15$.

From Fig. 9 can be concluded that $\dot{\sigma}_c$, the stress rate that is counterbalancing the stress relaxation rate is equal to the initial stress rate $\dot{\sigma}_0$ in the

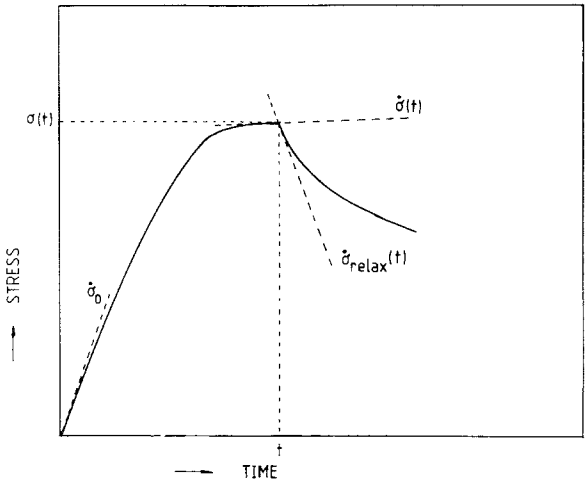

Fig. 8. Stress versus time during a typical stress relaxation experiment on UHMWPE fibers. $\dot{\sigma}_0$: initial stress rate, $\dot{\sigma}(t)$: actual stess rate at time t, $\dot{\sigma}_{\text{relax}}(t)$: immediate stress relaxation rate at time t

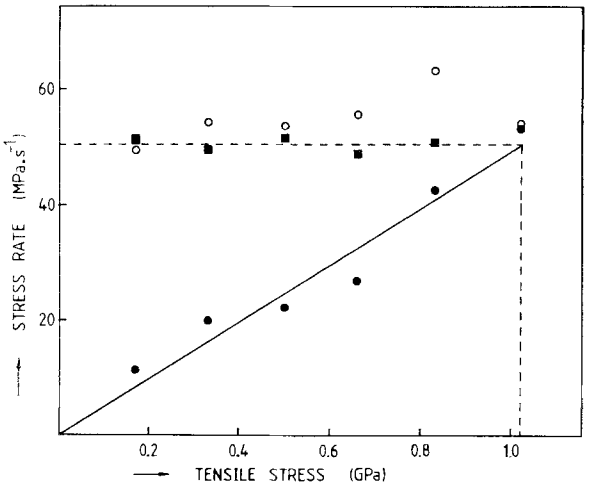

Fig. 9. Stress rates versus tensile stress of an UHMWPE fiber ($\lambda = 15$, 2.5 wt.% Hifax B). ■: $\dot{\sigma}_0$, ○: $\dot{\sigma}_c$, ●: $|\dot{\sigma}_{\text{relax}}|$

loading curve. The initial stress rate can be converted into a modulus E_0 using

$$E_0 = \frac{\dot{\sigma}_0}{\dot{\varepsilon}} . \tag{4}$$

In this case, one obtains an initial modulus of 30.2 GPa. The fact that $\dot{\sigma}_c = \dot{\sigma}_0$ is in accordance with the Boltzmann superposition principle [30]. Suppose that during simple extension the tensile stress is some function of time:

$$\sigma(t) = f(t) . \tag{5}$$

The process of stopping the crosshead at time t_0, can be considered as the result of applying a strain rate of the same magnitude, but oppositely directed, so that the net strain rate is zero. The stress during relaxation after t_0 would then be described by:

$$t \geq t_0: \quad \sigma_{\text{relax}}(t) = f(t) - f(t - t_0) . \tag{6}$$

By taking the time derivative of (6) and inserting $t = t_0$, one obtains:

$$t = t_0: \quad \dot{\sigma}_{\text{relax}}(t_0) = \dot{f}(t_0) - \dot{f}(0) . \tag{7}$$

Evaluating Eq. (3) at time t_0 and comparing it to Eq. (7), it immediately follows that $\dot{\sigma}_c = \dot{\sigma}_0$, which has been found from Fig. 9. In physical terms, it must be concluded that for a yielding fiber, as shown in Fig. 9, the morphology that accounts for the initial modulus is still present during the yielding process. The plastic flow during deformation of the fiber under these conditions does not affect the morphological element that determines the elastic properties, i.e., the initial modulus. It should be noted that under other conditions, where extensive yielding may take place, deviations from Eq. (7) can occur due to structural rearrangements upon yielding (strain softening/hardening).

Another result from Fig. 9 is that, roughly, the following relation seem to be valid:

$$|\dot{\sigma}_{\text{relax}}| = a \cdot \sigma , \tag{8}$$

where a is some constant. In this case, $a = 0.048\ \text{s}^{-1}$. Equation (8) is also a property of an ordinary Maxwell element [11, 13, 31] and, therefore, it can be stated that:

$$a = \frac{1}{\tau} , \tag{9}$$

where τ is the relaxation time of the dashpot. From (9), a relaxation time of 20.8 s can be calculated.

The horizontal dashed line in Fig. 9 is the mean value of $\dot{\sigma}_0$, the vertical one is the tensile strength (yield stress). It is clear from Fig. 9 that this yield stress is determined by the intercept of $|\dot{\sigma}_{\text{relax}}|$ and the mean value of $\dot{\sigma}_0$. In other words, the yield stress is reached when the absolute value of the stress relaxation rate equals the initial stress rate, i.e., the increase of stress due to stretching of elastic elements. When these two stress rates are equal the net stress rate is zero and stress is not increased during elongation. The tensile strength is therefore limited by flow (ductile fracture). The yield stress can be calculated from the initial modulus using Eq. (8):

$$\text{yielding:} \quad |\dot{\sigma}_{\text{relax}}| = a \cdot \sigma_{\text{yield}} = \dot{\sigma}_0$$

$$\rightarrow \sigma_{\text{yield}} = \frac{\dot{\sigma}_0}{a} . \tag{10}$$

From (10), using $\dot{\sigma}_0 = 50.3\ \text{MPa} \cdot \text{s}^{-1}$ and $a = 0.048\ \text{s}^{-1}$, a yield stress of 1.05 GPa can be calculated, which is equal to the experimental tensile strength.

Different behavior is found when a fiber of $\lambda = 60$ from a 2.5 wt.% gel is subjected to the same analysis (Fig. 10). This fiber does not yield, it has a low strain at break ($\sim$ 3.5%), and a much higher modulus (160 GPa). Again, it can be concluded from Fig. 10 that $\dot{\sigma}_c = \dot{\sigma}_0$ and that $|\dot{\sigma}_{\text{relax}}| = a \cdot \sigma$. From Fig. 10 $a = 0.026\ \text{s}^{-1}$ ($\tau = 38$ s). Although this value differs from that determined for the

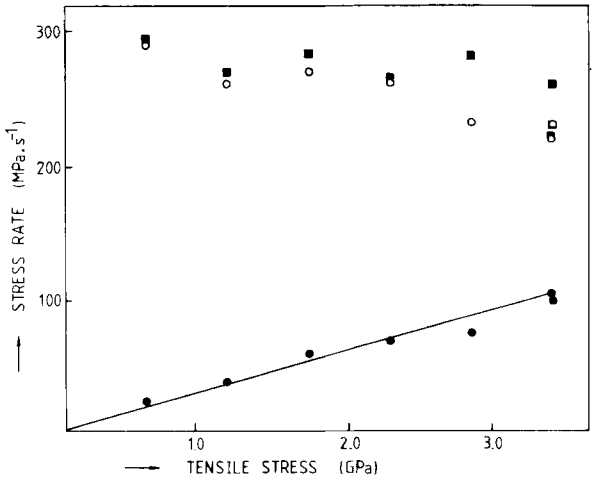

Fig. 10. Stress rates versus tensile stress of an UHMWPE fiber ($\lambda = 60$, 2.5 wt.% Hifax B). ■: $\dot{\sigma}_0$, ○: $\dot{\sigma}_c$, ●: $|\dot{\sigma}_{\text{relax}}|$

$\lambda = 15$ fiber, it can be concluded that this relaxation constant a does not change very much as a function of morphology and the moduli of the fibers differ by about a factor of 5 (difference in draw ratio 4 times).

The most striking difference between Figs. 9 and 10 is the fact that, in Fig. 10, $|\dot{\sigma}_{\text{relax}}|$ at the tensile stress at break (3.5 GPa) is still much lower than $\dot{\sigma}_0$. This means that the tensile strength in this case is not limited by flow: the fiber displays brittle fracture. The theoretical yield stress for this fiber can, however, still be calculated using Eq. (10). With $\dot{\sigma}_0 = 268$ MPa $\cdot$ s^{-1} and $a = 0.026$ s^{-1}, one obtains $\sigma_{\text{yield}} = 10.3$ GPa. The ratio between the experimental tensile strength and the yield stress is therefore 0.34. From Figs. 9 and 10 it can be concluded that stress relaxation is always present, both in high and low modulus fibers. The immediate stress relaxation rate is directly proportional to the applied tensile stress. For a given deformation rate and temperature only the modulus E_0 then determines the tensile strength (yield stress) because Eq. (10) can be rewritten as:

$$\sigma_{\text{yield}} = \frac{\dot{\sigma}_0}{a} = \frac{\dot{\varepsilon}}{a} \cdot E_0 \,. \tag{11}$$

The consequence of Eq. (11) is that the ratio of modulus and yield stress ($E_0/\sigma_{\text{yield}}$) is a constant ($a/\dot{\varepsilon}$) for given deformation rate and temperature. This value is respectively 29 and 16 for fibers shown in Figs. 9 and 10. Similar observations have already been reported for a variety of polymers [32], and our values compare well with values found for most textile fibers [33]. Buchdahl derived this relation by using the criterion of mechanical instability in shear [32]. Equation (11) is, in fact, similar to expressions for theoretical shear stresses of crystals [34].

From Fig. 10, we see that fibers having higher moduli already may break below the yield stress in a brittle manner. The stress relaxation process, however, is still occurring in these fibers, but it does not limit the tensile strength. As the modulus of fibers increases, there is a change-over from ductile to brittle fracture.

On the basis of the time-temperature superposition principle, it can be expected that at higher deformation rates, i.e., lower temperatures, the stress relaxation process slows down. This is demonstrated in Fig. 11, where $|\dot{\sigma}_{\text{relax}}|$ and the relaxation modulus $|\dot{\sigma}_{\text{relax}}|/\dot{\varepsilon}$ are plotted vs crosshead speed. Here a $\lambda = 25$ fiber from a 6.0 wt.% gel was strained at every crosshead speed up to a stress of 2.25 GPa. The value of $|\dot{\sigma}_{\text{relax}}|$ increases strongly with increasing crosshead speed, also indicating that the stress relaxation is not caused by slip through the action grips. The relaxation modulus, however, decreases with increasing crosshead speed, as would be expected for lower temperatures. The next step would be to examine whether one can see the ductile to brittle transition as a function of crosshead speed. In Fig. 12 the initial modulus and the relaxation modulus close to the tensile strength are plotted vs crosshead speed for the same fiber as in Fig. 9. The initial modulus varies somewhat, but this must be attributed to non-homogeneity of the fiber. The relaxation modulus close to the tensile strength is at low crosshead speed significantly higher than the initial modulus. Probably, strain hardening is taking place before break. At higher crosshead speeds the relaxation modulus close to the tensile strength goes down rapidly and becomes lower than the initial modulus. From the corresponding stress-strain curves, yielding fibers are observed at the low crosshead speeds, and as the speed increases a change-over to lower strains at break can be observed (brittle fracture).

The tensile stress of the fiber as a function of crosshead speed is given in Fig. 13. The ductile-to-brittle transition is accompanied by a change in the dependence of the tensile strength on the crosshead

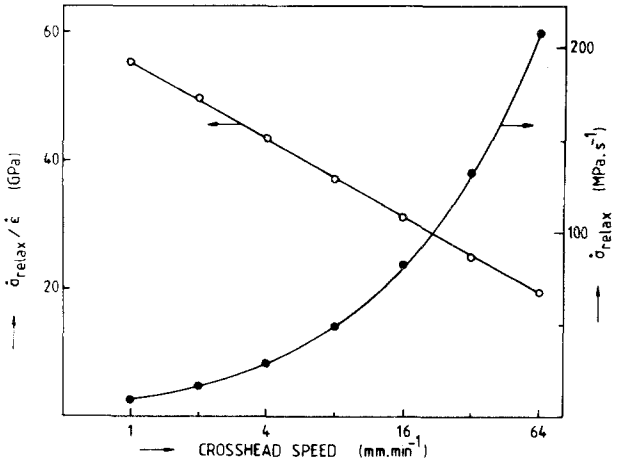

Fig. 11. Stress relaxation rate and relaxation modulus versus crosshead speed of a UHMWPE fiber ($\lambda = 25$, 6.0 wt.% Hifax B) at a tensile stress of 2.25 GPa. ●: $|\dot{\sigma}_{\text{relax}}|$, ○: $|\dot{\sigma}_{\text{relax}}|/\dot{\varepsilon}$. Sample length 100 mm

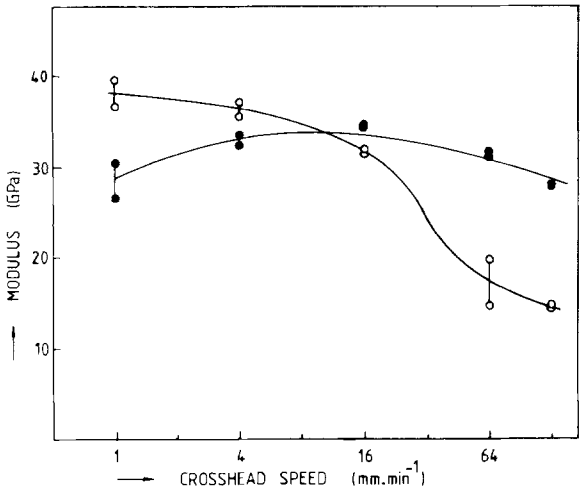

Fig. 12. Relaxation modulus at tensile strength and initial modulus versus crosshead speed of a UHMWPE fiber ($\lambda = 15$, 2.5 wt.% Hifax B) illustrating the ductile-to-brittle transition. ●: $\dot{\sigma}_0$, ○: $|\dot{\sigma}_{relax}|/\dot{\varepsilon}$. Sample length 100 mm

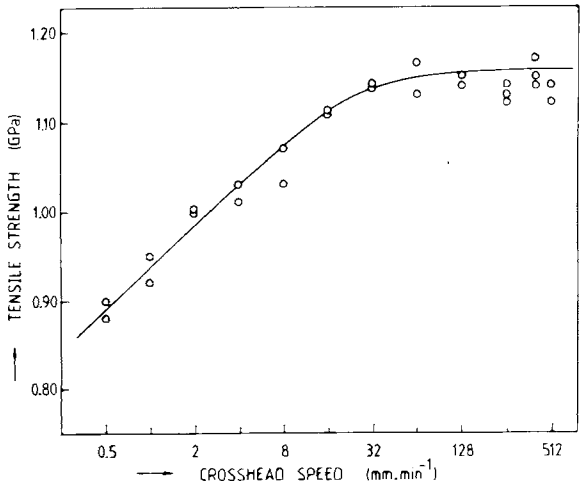

Fig. 13. Tensile strength versus crosshead speed of a UHMWPE fiber ($\lambda = 15$, 2.5 wt.% Hifax B) showing the ductile to brittle transition. Sample length 28 mm

speed. In the ductile region the tensile strength increases significantly with increasing crosshead speed [35]. In the brittle region, however, the slope of the line goes down strongly and also more scatter is observed. According to Eyring's theory of flow [13], the strain rate can be written as:

$$\dot{\varepsilon} = A \cdot \exp\left\{ -\frac{U_0 - \gamma \cdot \sigma}{RT} \right\}, \tag{12}$$

where A is a constant of order of kT/h, U_0 is the activation energy, and γ the activation volume. Therefore, the yield stress σ_{yield} can be written as:

$$\sigma_{yield} = \frac{U_0}{\gamma} + \frac{RT}{\gamma} \cdot \ln \dot{\varepsilon} - \frac{RT}{\gamma} \cdot \ln A \,. \tag{13}$$

According to this, the slope at the lefthand side in Fig. 13 must be equal to RT/γ, where γ is the activation volume. In this case, an activation volume of 66 Å^3 for plastic flow can be calculated. Kubát [36] has shown from studies on different materials that the activation volume in stress relaxation is:

$$\gamma \approx 10 \cdot \frac{kT}{\sigma^*}, \tag{14}$$

where σ^* is the effective stress (applied stress minus internal stress). If one neglects internal stresses, an activation volume of 48 Å^3 can be calculated from Eq. (14), using $\sigma = 0.85$ GPa. This is within reasonable agreement with the value of 66 Å^3, especially if one considers that by neglecting internal stresses in the calculation, a systematically lower value of γ is obtained. The very small volume of 66 Å^3 comes down to a chain segment of about 3 monomeric units. Wilding and Ward [15] have found activation volumes ranging from 50 to 87 Å^3 for creep in different polyethylene samples.

It needs to be emphasized that the Eyring equation (12) implies several assumptions, as has been pointed out by White who has developed and applied a modified theory [37, 38]. Application of the White theory is beyond the scope of the present investigation, but it clearly shows that the activation volume, as determined here, can be interpreted with some difficulty, but in a straightforward way. The activation volume is calculated here only for comparison.

In a recent study [10] the temperature dependence of the tensile strength has been investigated. The tensile strength vs temperature is plotted in Fig. 14 for a $\lambda = 100$ fiber from a 5.0 wt.% Hifax A gel. A similar ductile-to-brittle transition was found as in Fig. 13. At temperatures above 20 °C the fibers increasingly exhibit yielding behavior and the tensile strength (yield stress) decreases linearly to zero at 152 °C. This is the temperature at which the orthorhombic crystal lattice transforms into the hexagonal phase. The existence of this solid-solid phase transition in UHMWPE fibers has been demonstrated by x-ray diffraction and differential scanning calorimetry [39]. This lattice transition is also

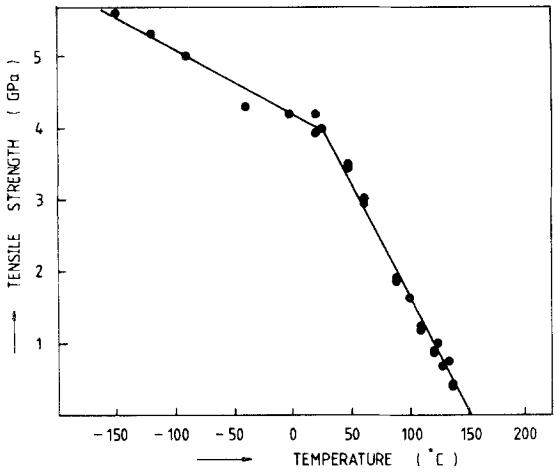

Fig. 14. Tensile strength versus tensile testing temperature of a UHMWPE fiber ($\lambda = 100$, 5.0 wt.% Hifax A) showing the ductile to brittle transition upon decrease of temperature (from [10]). At 152 °C orthorhombic crystalline material transforms into the hexagonal phase. Crosshead speed 10 mm/min, sample length 50 mm

well known for *n*-paraffins and polyethylene crystallized under high pressures. A complete review of this phenomenon occurring in a variety of solids was recently given by Wunderlich et al. [40]. The hexagonal rotator phase of polyethylene exhibits conformational disorder. The chains in such a phase have an especially high mobility and can easily slip past each other.

Comparing the result of the temperature study on the tensile strength and the results on stress relaxation as presented in this work, it can be concluded that stress relaxation is strongly linked to orthorhombic-hexagonal phase transition. Stress could be relaxed by the slipping of chains past each other inside the crystal lattice. In general, flow in UHMWPE fibers can be thought to be caused by local solid-solid transitions inside crystalline entities and not by flow of amorphous domains. This would also account for the very small activation volume of 66 $Å^3$. Wide angle x-ray experiments on fibers subjected to creep, however, have not demonstrated the presence of the hexagonal phase next to the orthorhombic. This means that stress does not induce a total phase transition of crystalline blocks. Local phase transitions not detectable by x-ray diffraction could still have taken place. Figure 14, nevertheless, clearly indicates the introduction of the hexagonal phase at lower temperatures under the action of the tensile stress.

In studies on other polymers, stress-induced phase transitions in fibers have been reported [41–43]. Niegisch [44] has observed for poly-(*p*-xylylene) that already below the melting point conformationally disordered phases similar to the hexagonal phase of polyethylene [45] are found and there are substantially higher creep rates in these phases.

Stress-strain relation

From the results on stress relaxation the stress-strain relation of UHMWPE fibers can be easily derived. It has been shown that the following relation is valid:

$$\dot{\sigma}(t) = \dot{\sigma}_0 - a \cdot \sigma = E_0 \cdot \dot{\varepsilon} - a \cdot \sigma \; . \tag{15}$$

Solving this differential equation, one obtains:

$$\sigma(t) = \frac{E_0 \cdot \dot{\varepsilon}}{a} \cdot (1 - e^{-a \cdot t}) \; . \tag{16}$$

Inserting $t = \varepsilon/\dot{\varepsilon}$, the stress-strain relation can be derived:

$$\sigma(\varepsilon) = \frac{E_0}{b} \cdot (1 - e^{-b \cdot \varepsilon}) \; , \tag{17}$$

where $b = a/\dot{\varepsilon}$.

The function in Eq. (17) is plotted in Fig. 15. Note that the stress asymptotically approaches the yield stress. Although the form of the function seems to describe most experimental stress-strain curves rather well, a simple test on the validity of Eq. (18) can be done as follows.

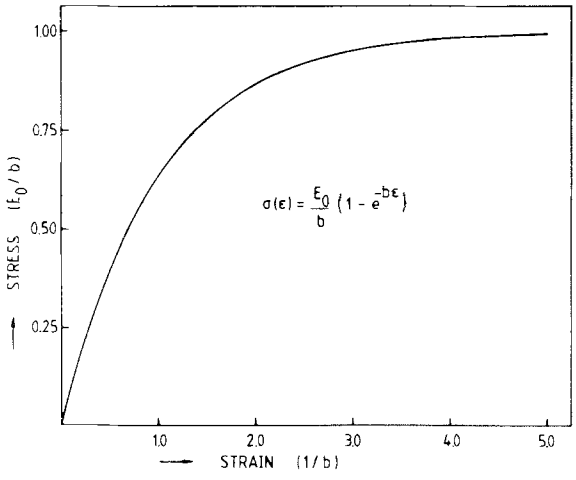

Fig. 15. General theoretical stress strain curve for gel-spun and hot-drawn UHMWPE fibers

From Eq. (17) the following relation can be derived for the tangent modulus E in a stress-strain curve as a function of tensile stress σ:

$$E(\sigma) = \frac{d\sigma}{d\varepsilon} = E_0 \cdot e^{-b \cdot \varepsilon} = E_0 - b \cdot \sigma \ . \qquad (18)$$

Therefore, if Eq. (17) is applicable, a plot of the tangent modulus vs stress should give a straight line with a negative slope. The slope of the line b can be directly related to the stress relaxation process and is a direct measure of the extent of plastic flow during deformation.

Such a plot is given in Fig. 16 for three very different fibers from Hifax B: $\lambda = 15$ (2.5 wt.% gel), $\lambda = 60$ (2.5 wt.% gel) and $\lambda = 170$ (1.5 wt.% gel). The latter has a very high initial modulus of 264 GPa. From Fig. 16 the linear decrease of the tangent modulus is clearly affirmed for the fiber. During tensile deformation the modulus decreases with increasing stress from 264 GPa to 119 GPa at the stress at break of 5.4 GPa. The fiber breaks in a brittle manner at a strain at break of 3.0%. Similar results are obtained for the $\lambda = 60$ (2.5wt.% gel) fiber. The $\lambda = 15$ (2.5 wt. % gel) fiber yields, and modulus therefore decreases close to zero. For this fiber, however, the decrease of the tangent modulus is less linear than for the higher modulus fibers. All three fibers in Fig. 16 have been strained by applying the same crosshead speed, temperature, and sample lengths. The slopes b for the fibers are: 28 ($\lambda = 170$), 22 ($\lambda = 60$), and 24 ($\lambda = 15$).

More precise modulus-stress plots can be obtained by calculations on digitized stress-strain data. Figure 17 shows stress-strain curves of three different fibers: $\lambda = 15$, $\lambda = 30$ and $\lambda = 70$ (1.5 wt.% gel). Figures 18 to 20 are the corresponding modulus-stress plots of these stress-strain curves. The modulus at a given point y in the stress-strain curve was determined from the slope of the least-squares fit through $(2N + 1)$ points ranging from $y - N$ to $y + N$.

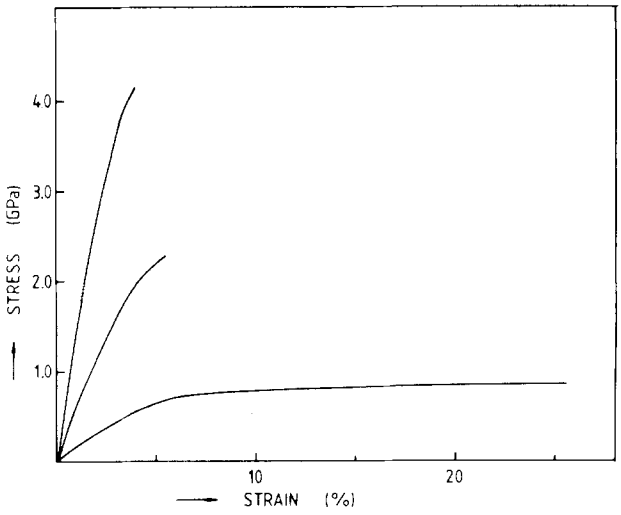

Fig. 17. Stress versus strain for $\lambda = 15$, $\lambda = 30$, and $\lambda = 70$ UHMWPE fiber (1.5 wt.% Hifax B). Sample length: 500 mm. Crosshead speed: 50 mm/min

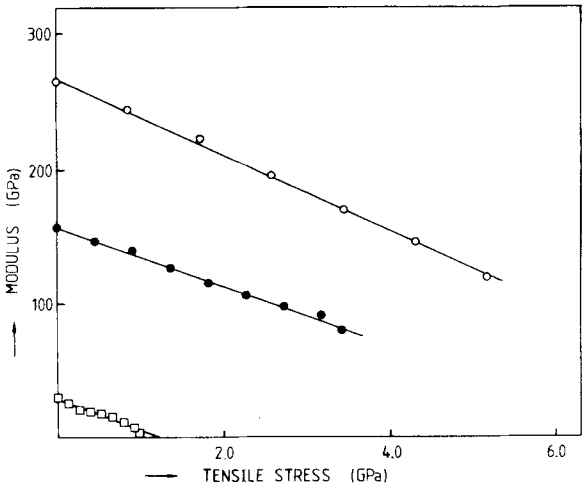

Fig. 16. Tangent modulus versus tensile stress of three different UHMWPE fibers. ○: $\lambda = 170$, 1.5 wt.% Hifax B; ●: $\lambda = 60$, 2.5 wt.% Hifax B; □: $\lambda = 15$, 2.5 wt.% Hifax B

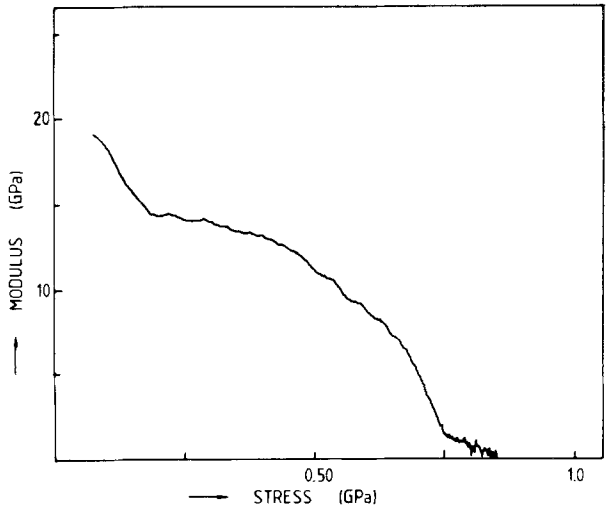

Fig. 18. Tangent modulus versus tensile stress for a $\lambda = 15$ UHMWPE fiber (see Fig. 17)

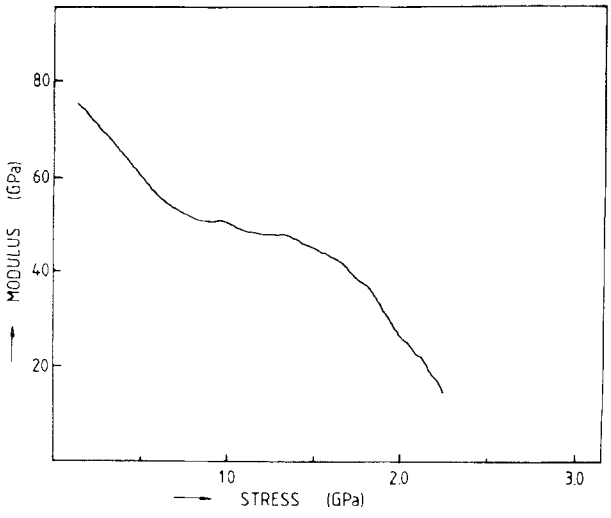

Fig. 19. Tangent modulus versus tensile stress for a $\lambda = 30$ UHMWPE fiber (see Fig. 17)

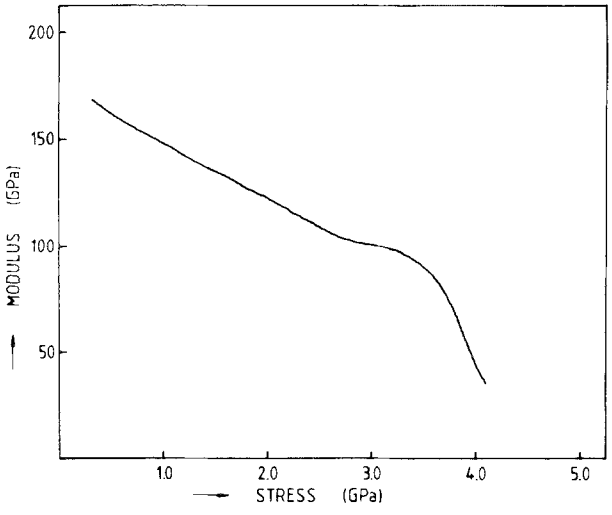

Fig. 20. Tangent modulus versus tensile stress for a $\lambda = 70$ UHMWPE fiber (see Fig. 17)

Especially Figs. 18 and 19 clearly show a nonlinear decrease of the modulus. By comparison of the three plots it can be seen that the plots can be divided into two distinct regions: a linear one at low stresses and a non-linear one at high stresses. The initial linear decrease of the modulus is most pronounced for the $\lambda = 70$ fiber, and this slope becomes steeper going to lower draw ratios (-26.1 ($\lambda = 70$), -43.9 ($\lambda = 30$) and -44.5 ($\lambda = 15$)). The transition point to the non-linear regions occurs for all three fibers after around 40% decrease of the initial modulus. The details of the modulus-stress plots are very reproducible and the curves are characteristic for the draw ratios of the fiber.

Considering the results as presented sofar, we can make a distinction between the contribution of elastic strain and plastic strain to the total tensile strain. The elastic strain at a given stress can easily be calculated by dividing the stress by the initial modulus. The difference between measured tensile strain at that stress and the elastic strain is the plastic strain, i.e., the elongation due purely to flow. These values are given in Table 1 for the three fibers shown in Figs. 17–20. The data show that plastic strain is a considerable contribution to the macroscopic strain at break. For the $\lambda = 70$ fiber plastic strain is 40% of the strain at break. From this, it must also be concluded that a large part of this plastic strain is directly reversible, because the hysteresis strain caused by cyclic deformation would normally be only 10% of the cyclic strain under these conditions.

The consequence of Eq. (15) is also that at every stress the initial modulus E_0 is present, but that the actual modulus is changed by a flow process. Using this concept the presence of negative stress relaxation [13] can be predicted. When performing a loading and unloading cycle, it is always found that the absolute tangent modulus at the end of the unloading curve is lower than the initial modulus, whereas the tangent at the beginning of the unloading curve is higher. This then should mean that in the first part of the unloading curve the tangent modulus is increased by stress relaxation. In the second part, however, a process that tends to increase stress in time has to be expected, because the value of the tangent modulus is lower than the initial modulus. This is indeed the case, as is shown in Fig. 21. At t_1, $|\dot{\sigma}(t_1)|$ is larger than $\dot{\sigma}_0$, and stress relaxation is present. At t_2 the absolute value of the tangent modulus is equal to $\dot{\sigma}_0$. At t_3, where $|\dot{\sigma}(t_3)|$

Table 1. Tensile strength σ_b, initial Young's modulus E_0, elastic strain at break $\varepsilon_{elastic}$, and plastic strain at break $\varepsilon_{plastic}$ of UHMWPE (1.5 wt.% Hifax B) fibers. Gauge length: 500 mm. Crosshead speed: 50 mm/min

Draw ratio	σ_b (GPa)	E_0 (GPa)	$\varepsilon_{elastic}$ (%)	$\varepsilon_{plastic}$ (%)
70	4.16	175	2.38	1.56
30	2.26	82.1	2.75	2.65
15	0.85	22.6	3.8	21.7

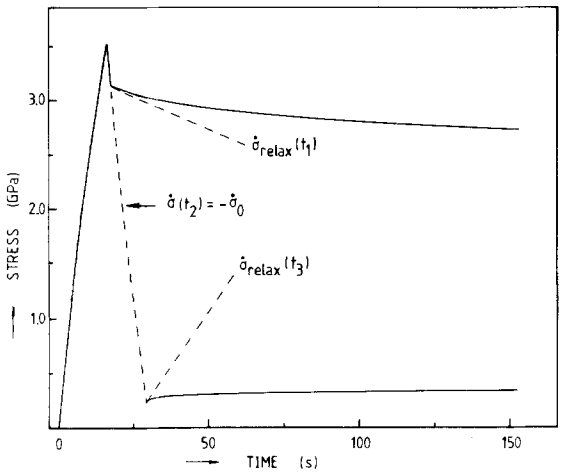

Fig. 21. Stress versus time during a deformation cycle of a UHMWPE fiber ($\lambda = 60$, 2.5 wt.% Hifax B). t_1: normal stress relaxation ($|\dot{\sigma}(t_1)| > \dot{\sigma}_0$), t_2: $|\dot{\sigma}(t_2)| = \dot{\sigma}_0$, t_3: negative stress relaxation ($|\dot{\sigma}(t_3)| < \dot{\sigma}_0$)

is lower than $\dot{\sigma}_0$, an oppositely acting process (negative stress relaxation) is indeed observed. This kind of behavior can be found in fibers from different polymers [46], and we have observed it even in fibers from very stiff polymers like poly(*p*-phenyleneterephtalamide). It should be noted that negative stress relaxation cannot be explained using the Boltzmann superposition principle in the simple way as described in Eqs. (5) to (7).

Proposed mechanism of flow in gel-spun and hot-drawn UHMWPE fibers

From the results in the previous sections, it can be concluded that flow plays a major role during tensile deformation of UHMWPE fibers. Furthermore, the process of flow was shown to be strongly correlated to the orthorhombic-hexagonal phase transition of crystalline material in UHMWPE fibers. Considering these results, the microscopic mechanism of flow, therefore, has to be a general and simple one.

Although it is very difficult to translate macroscopical properties of fibers into molecular processes due to the extreme complexity of the fiber morphology of flexible chain polymers, an attempt will be made to describe the mechanism of flow in these fibers using the generally accepted model for high strength and high modulus UHMWPE fibers, as shown in Fig. 22. This model can be used to

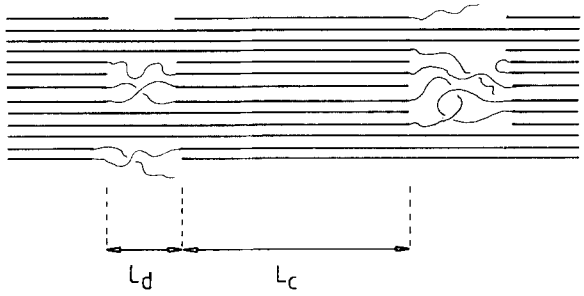

Fig. 22. Schematic representation of an elementary microfibril in gel-spun and hot-drawn UHMWPE fibers, showing crystalline blocks with length L_c and disordered domains with length L_d

quantitatively describe the seemingly puzzling combination of high crystallinity (about 90%), high modulus (about 75% of the ultimate modulus of around 350 GPa [24, 47]), and the relatively low strain at break of 3–4% and tensile strength of maximally 7.2 GPa (theoretically, 21% and 33 GPa, respectively [33, 48]) encountered in UHMWPE fibers [49].

As shown in Fig. 22 the fiber consists of crystalline blocks that are connected by tie molecules. The fraction of tie molecules per surface area directly determines the tensile strength [50], whereas the elastic modulus and the strain at break depend on both the fraction of tie molecules and the ratio of the length L_c of the crystalline block to the length L_d of the disordered domain, through which the tie molecules pass [49]. Flow in such a morphology could be described as follows.

As has been shown, flow is very general for all UHMWPE fibers and is most likely not caused by motion of large chain sections in the more amorphous parts of the fiber morphology (the disordered domain). This is also reflected in the small activation volume of about 3 monomeric units. Upon tensile deformation, tensile stress is concentrated on the tie molecules. The bond angles of the backbone of the molecules are increased and the carbon and hydrogen atoms of the all-trans chain move closer to the imaginary chain axis of the corresponding molecule. Due to this, the interaction forces between atoms in neighboring chains decrease drastically with elongation of the chains, because the distance between the atoms has increased. In polyethylene, the interaction force is solely determined by weak van der Waals interactions that very rapidly decrease to a negligible

level with increasing interaction distance. Beyond a certain critical elongation, the chains can then easily slip past each other. This comes down to a stress-induced transition from the orthorhombic to the hexagonal phase. The tie molecules, however, are fixed at both ends in crystalline blocks, in which the bond angles of the polymer chains are only slightly increased due to the lower stress level. Under influence of the concentrated stress on each individual tie molecule and promoted by thermal motions the chain part of the tie molecules inside the crystalline blocks will be slowly pulled out, resulting in elongation of the fiber. Calculations on the static and thermally activated displacements of chains against a crystal lattice have been reviewed by Kausch [9].

Flow can thus be thought to be caused by the gradual pull-out of tie molecules out of crystalline blocks and that this process is identical to localized transitions inside crystalline blocks from the orthorhombic to the hexagonal phase.

This process of flow can be expected to be largely reversible on a small timescale. Partially pulled-out chains can be pulled back again into their original position. The driving force for this is the lattice mismatch of pulled-out chain with the surrounding crystalline block and the presence of residual stresses, causing recrystallization after removal of the tensile stress. This is consistent with observations that upon tensile deformation plastic strains are considerable even at low strain levels, as the data in the Table 1 show, but that it nevertheless can be largely reversed during unloading. Total reversal of the slip process may be achieved only after a long period of time, as has been discussed earlier. Changes in density of ultra-high molecular weight linear polyethylene have been reported even after storage of about 100 days at room temperature [51], demonstrating long-time crystallization events.

The thermophysical behavior during deformation, as was pioneered for polymers by Müller [52], was investigated for polyethylene by Godovsky and other Russian researchers [53]. They found that oriented polyethylene releases heat during elongation, which is a result from the negative coefficient of thermal expansion. Contraction, however, again caused an initial release of heat, but was then followed by absorption of heat (as must be expected during contraction from the negative coefficient of thermal expansion). This result is indicative of a reversible slip process during cyclic deformation, and is consistent with our proposed mechanism.

At larger strains another process has to come into action, because the process described sofar cannot explain extensive yielding leading to tensile strains on the order of the initial sample length. It is conceivable that, while chains start to slip out of a crystalline block at a large number of different sites, at a given moment the coherence will be lost inside the crystalline block (stress-induced melting), and separate flow of bundles of chains (microfibrils) will occur and these will slip past each other. Such a process may lead to unfolding of remaining lamellar material or extensive microfibrillar slip and can explain the yielding over large strains, even for fully oriented fibers. Once this process starts, flow will become irreversible and plastic deformation sets in. The fiber structure then is drastically changed by flow and, after deformation, the morphology will settle down in new local energy minima.

The modulus-stress plots in Figs. 18–20 indeed show two regions. If the first linear region is attributed to the pull-out of chains, it is then consistent to find that for higher draw ratios this region becomes more prominent due to the increased length of the crystalline blocks. The transition to a second non-linear region could then be the onset of microfibrillar slip.

The proposed mechanism of flow comes down to stress-induced melting. Fibers of polymers having high melting points should therefore be less susceptible to flow at a given stress and temperature. Figure 23 shows the strain vs time during a creep experiment, at room temperature, of a poly(*p*-xylylene) (PPX) fiber (for preparation see [54]) and a UHMWPE fiber, both having a tensile strength of 2.3 GPa. The load corresponds in both cases to 60% of the load at break. The plot shows clearly the extensive flow and the short time to break (1 h) of the UHMWPE fiber. The PPX fiber responds profoundly differently and does not show any increase of strain after being loaded within the accuracy of the experimental set-up (0.1% strain).

The high resistance to flow in PPX fibers is also demonstrated by stress relaxation. Figure 24 shows the stress, as a percentage of the stress at which the crosshead was stopped, versus log(time) of a PPX and a UHMWPE fiber. Both fibers had been elongated up to a tensile stress which corresponded to

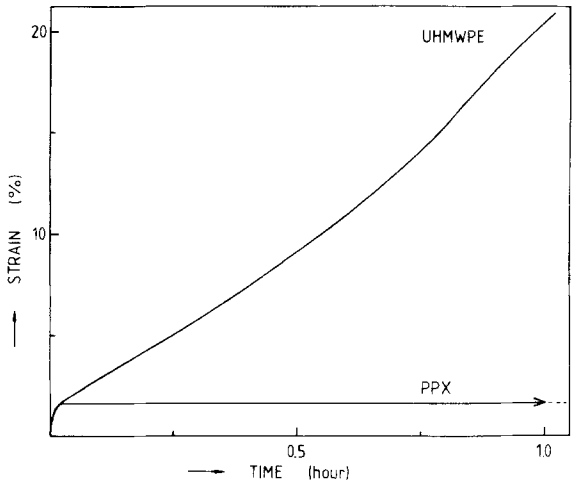

Fig. 23. Strain versus time of PPX and UHMWPE (1.5 wt.% Hifax B) fibers during a dead-load test. Both fibers, having a tensile strength of 2.3 GPa, had loads attached corresponding to 60% of the load at break

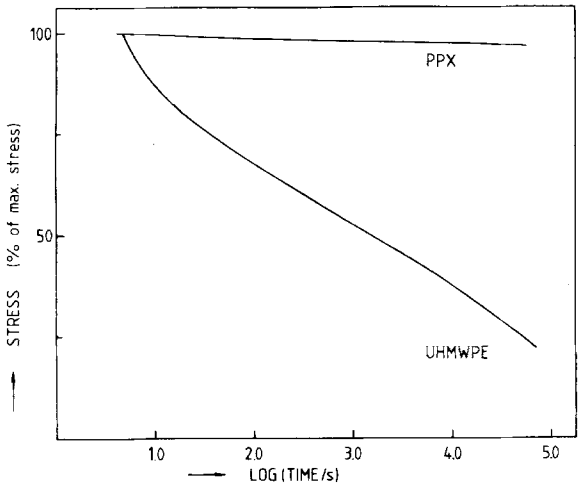

Fig. 24. Stress versus log(time) during stress relaxation of PPX and UHMWPE (1.5 wt.% Hifax B) fibers. Both fibers were stressed up to 60% of their tensile strengths (2.1 GPa and 2.3 GPa, respectively). Crosshead speed: 10 mm/min. Zero time corresponds to the start of the crosshead movement

60% of the stress at break. The UHMWPE fiber again shows the ease of flow in these fibers, for it relaxes over 75% of the initial stress during 17.4 h, whereas the PPX fiber is able to relax only 3.6% of its initial stress.

Both PE and PPX are pure hydrocarbon polymers, with no permanent dipoles and no possibility of hydrogen bonding between chains. Heat of fusion is 292 J/gr for PE [55] and 159 J/gr for PPX (including mesomorphic transitions) [45]. The melting point, determined by the heat and entropy of fusion, however, is 142 °C for PE [55] and 427 °C for PPX [45]. This indicates that melting, i.e., disruption of a crystalline block under tensile stress is much easier to introduce in a UHMWPE fiber than in a PPX fiber.

4. Conclusions

Cyclic deformations and analysis of the deformation energetics have shown that during tensile deformation up to break of gel-spun and hot-drawn UHMWPE fibers, no detectable amount of deformation energy is used to break chemical bonds in the polymeric chain. Flow processes, as demonstrated by dissipation of deformation energy, creep, and stress relaxation are predominantly present in addition to elastic processes. In high modulus UHMWPE fibers having a strain at break of 3–4%, this flow process is reversible, because initial stress-strain behavior can be recovered after a cyclic deformation.

From stress relaxation experiments it was found that the immediate stress relaxation rate after deformation is directly proportional to the applied tensile stress. The proportionality is affected by the deformation rate. In accordance with the Boltzmann superposition principle, the curvature in a stress-strain curve could be described as the result of the elastic modulus and the stress relaxation modulus. The stress relaxation process was used to describe the ductile-to-brittle transition of UHMWPE fibers as a function of deformation rate. Combining this result with those from studies on the tensile strength as a function of temperature, it was shown that the process of flow is strongly correlated to the orthorhombic-hexagonal phase transition of crystalline material in UHMWPE fibers. On the basis of the results on stress relaxation, a phenomenological stress-strain relation for UHMWPE fibers could be derived. From this relation – identical to the stress-strain relation of a simple Maxwell element – the linear dependence of yield stress upon modulus can be directly derived. Experimental stress-strain curves of, especially, highly drawn UHMWPE fibers can be quite accurately described by the derived relation, but indicate the presence of different flow processes during tensile deformation. Using the general morphological

model for UHMWPE fibers, a mechanism of flow was proposed in which, at first, flow is caused by pull-out of molecules (tie molecules, intercrystalline bridges) from crystalline blocks, followed by the destruction of crystalline blocks through slip of microfibrils past each other (stress-induced melting). The experimental data can be qualitatively described by this mechanism.

Acknowledgements

The contributions of J. P. Penning and M. Roukema to the fiber preparation are gratefully acknowledged. This study was supported by the Netherlands Foundation of Chemical Research (SON), with financial aid from the Netherlands Organization for the Advancement of Pure Research (NWO) and AKZO, The Netherlands.

References

1. Kalb B, Pennings AJ (1980) J Mat Sci 15:2584
2. Smith P, Lemstra PJ, Kalb B, Pennings AJ (1979) Polym Bull 1:733
3. Smook J, Flintermann M, Pennings AJ (1980) Polym Bull 2:775
4. Hoogsteen W, Kormelink H, Eshuis G, ten Brinke G, Pennings AJ (1988) J Mat Sci 23:3467
5. Pennings AJ, Roukema M, van der Veen A (1990) Polym Bull 23:353
6. Zhurkov SN, Narzullayev BN (1953) Zhur Tekh Fiz 23:1677
7. Bueche F (1955) J Appl Phys 26:1133
8. Tobolsky A, Eyring H (1943) J Chem Phys 11:125
9. Kausch HH (1987) Polymer fracture, polymer/properties and applications 2, second ed. Springer Verlag, Berlin Heidelberg
10. Dijkstra DJ, Torfs JCM, Pennings AJ (1989) Colloid Polym Sci 267:886
11. Ferry JD (1970) Viscoelastic properties of polymers, second ed. John Wiley & Sons
12. Pennings AJ, van der Hooft RJ, Postema AR, Hoogsteen W, ten Brinke G (1986) Polym Bull 16:167
13. Krausz AS, Eyring H (1975) Deformation kinetics. John Wiley & Sons
14. Wilding MA, Ward IM (1978) Polymer 19:969
15. Wilding MA, Ward IM (1981) Polymer 22:870
16. Smook J, Pennings AJ (1982) J Appl Polym Sci 27:2209
17. Frank O, Wendorff JH (1981) Colloid Polym Sci 259:1047
18. Frank O, Wendorff JH (1988) Colloid Polym Sci 266:216
19. Stoeckel TM, Blasius J, Crist B (1978) J Polm Sci Polym Phys Ed 16:485
20. Zwijnenburg A, Pennings AJ, unpublished results
21. Hoogsteen W, ten Brinke G, Pennings AJ (1990) J Mat Sci 25:1551
22. Zhurkov SN, Zakrevskyi VA, Korsukov VE, Kuksenko VS (1972) J Polym Sci Part A-2:10
23. Noether HD, Whitney W (1973) Kolloid Z Z Polym 251:991
24. Fanconi B, Rabolt JF (1985) J Polym Sci Polym Phys Ed 23:1201
25. Ward IM, Wilding MA (1984) J Polym Sci Polym Phys Ed 22:516
26. Kubát J, Seldén R, Righdahl M (1978) J Appl Polym Sci 22:1715
27. Kubát J (1979) Makromol Chem Suppl 3:233
28. Seldén R (1979) J Mat Sci 14:312
29. Hagström B, Kubát J, Rigdahl M (1988) J Appl Polym Sci 36:1375
30. Chang FSC (1964) J Appl Polym Sci 8:37
31. Williams JG (1973) Stress analysis of polymers. Longman, London
32. Buchdahl R (1958) J Polym Sci 28:239
33. Prevorsek DC (1966) J Polym Sci Part A-2 4:63
34. Kelly A, MacMillan NH (1986) Strong solids. Clarendon Press, Oxford
35. Schwartz P, Netravali A, Sembach S (1986) Text Res J 56:502
36. Kubát J (1965) Nature 205:378
37. White JR (1981) J Mat Sci 16:3249
38. Haworth B, White Jr (1981) J Mat Sci 16:3263
39. Pennings AJ, Zwijnenburg A (1979) J Polym Sci Polym Phys Ed 17:1011
40. Wunderlich B, Möller M, Grebowicz J, Baur H (1988) Adv Polym Sci 87
41. Ward IM, Wilding MA, Brody H (1976) J Polym Sci Polym Phys Ed 14:263
42. Jakeways R, Smith T, Ward IM, Wilding MA (1976) J Polym Sci Polym Lett Ed 14:41
43. Brereton MG, Davies GR, Jakeways R, Smith T, Ward IM (1978) Polymer 19:17
44. Niegisch WD (1966) J Appl Phys 37:4041
45. Kirkpatrick DE, Wunderlich B (1985) Makromol Chem 186:2595
46. Nachane RP, Hussain GFS, Patel GS, Krisha Iyer KR (1989) J Appl Polym Sci 38:21
47. McCullough RL, Eisenstein AJ, Weikart DF (1977) J Polym Sci Polym Phys Ed 15:1837
48. de Boer JH (1936) Trans Faraday Soc 32:10
49. Dijkstra DJ, Pennings AJ (1988) Polym Bull 19:73
50. Penning JP, van der Werff H, Roukema M, Pennings AJ (1990) Polym Bull 23:347
51. Alamo RG, McLaughlin KW, Mandelkern L (1989) Polym Bull 22:299
52. Müller FH (1969) In: Eirich (ed) Rheology, vol 5, ch. 8. Wiley, New York
53. Godovsky YuK (1982) Colloid Polym Sci 260:461 and references therein
54. van der Werff H, Pennings AJ (1988) Polym Bull 19:587
55. Wunderlich B, Czorny G (1977) Macromolecules 10:906

Received April 15, 1991;
accepted May 23, 1991

Authors' address:

Prof. Dr. A. J. Pennings
Department of Polymer Chemistry
University of Groningen
Nijenborgh 16
9747 AG Groningen, The Netherlands